PDMS/Polyimide Composite as an Elastomeric Substrate for Multifunctional Laser-Induced Graphene Electrodes

PDMS/Polyimide composite as elastomeric substrate for multifunctional laser-induced graphene electrodes

Matteo Parmeggiani[a,b], Pietro Zaccagnini[a,b], Stefano Stassi[b], Marco Fontana[a,b], Stefano Bianco[b], Carmelo Nicosia[b], Candido F. Pirri[a,b], Andrea Lamberti[a,b]*

[a]*Istituto Italiano di Tecnologia, Center for Sustainable Future Technologies, Corso Trento, 21, 10129 Torino, Italy*
E-mail: andrea.lamberti@polito.it

[b]*Politecnico di Torino, Dipartimento di Scienza Applicata e Tecnologia (DISAT), Corso Duca Degli Abruzzi, 24, 10129 Torino, Italy*

Keywords: PDMS composite, polyimide powder, laser-induced graphene, supercapacitors, strain sensors

Abstract

Laser-induced graphene (LIG) emerged as one of the most promising materials for flexible functional devices. However, the attempts to obtain LIG onto elastomeric substrates never succeed hindering its full exploitation for stretchable electronics. Herein a novel polymeric composite is reported as starting material for the fabrication of graphene-based electrodes by direct laser writing. A polyimide (PI) powder is dispersed into polydimethylsiloxane (PDMS) matrix in order to achieve an easily processable and functional elastomeric substrate allowing for the conversion of the polymeric surface into laser-induced graphene (LIG). The mechanical and electrical properties of the proposed material can be easily tuned by acting on the polyimide powder concentration. The reported procedure takes advantage from the simple casting process typical of silicone elastomer allowing to produce electrodes conformable to any kind of shape and surface as well as complex three-dimensional structures. Electrochemical capacitors and strain gauges are selected as flexible prototypes to demonstrate the multifunctional properties of the obtained LIG on PDMS/PI composite substrate.

1. Introduction

The field of flexible electronics is developing rapidly resulting in an increase in the demand for suitable materials for device fabrication.[1] The two main limitations are related to the production of flexible electrodes able to effectively work under bending and stretching condition and to the processability of these materials.[2] Several works in the literature report on materials with good performance of combined elasticity and conductivity; however these advantages are usually obtained through very complex fabrication processes and patterning strategies[3] or non-environmental friendly synthesis of active materials.[4]

Laser induced graphene (LIG) was recently proposed as a possible candidate for the fabrication of several kinds of flexible electronic devices thanks to the high mechanical stability and good electrical properties.[5] It has been extensively studied as electrode-material for flexible supercapacitors,[6-9] sensors,[10-11] environmental[12] and electro-catalyst applications.[13-14]

It consists of a three-dimensional network of few layer graphene (FLG) obtained by a laser writing process of the polymeric surface. The pioneering work by Tour and co-workers proposed a graphenization mechanism of polymer strongly correlated to the structural features present in the repeat units, in particular aromatic and imide repeat units.[15] The authors tried to generalize this laser-induced graphitization process by testing different polymers and their results show that only two polymers incur in graphenization, namely polyimide (PI) and poly(etherimide), both of which contain the aforementioned repeat units. We then demonstrated that this graphenization process could be possible also onto sulfonated poly(ether ether ketone) (SPEEK) and we shed light on this process by proposing a different and more detailed mechanism for LIG formation on SPEEK.[6] Afterwards, Tour and coworkers demonstrated that the laser graphenization can be extended to several other

polymers or organic precursor depending on the laser writing parameters and the gaseous environment.[16]

The proposed materials presented a high flexibility, but cannot be stretched since they have a high Young's modulus. Up to now there is a lack in the fabrication of stretchable electrodes with this approach since laser graphenization of elastomeric polymer has still not been demonstrated. Recently we have proposed a method to obtain LIG embedded into PDMS matrix by peeling the graphene network from a laser-written PI support.[17] We found this process to have some limitations both from the preparation and exploitability point of view. Indeed, PDMS infiltration into LIG network has a strong influence on the obtained LIG/ PDMS, since it requires long time and vacuum evacuation of trapped bubbles, affecting the PDMS casting onto curved surfaces and reducing the conductivity of the starting LIG on PI. In order to overcome the above mentioned issues, we propose a PDMS/PI powder composite as substrate to be laser-written: the uncured mixture can be easily casted on any kind of surface and, after cross-linking, it subsequently undergoes the typical graphenization process of polyimide during CO_2-laser writing. Moreover, the proposed material introduces the possibility to tune its mechanical and electrical properties by simply varying PI powder concentration. This feature allows to opportunely design the material properties as a function on the final application. In order to demonstrate the applicability of our approach we fabricated two flexible devices, a strain gauge and a supercapacitor, with different mechanical and electrical properties suitable to maximize the respective efficiencies.

2. Experimental Section

PDMS/PI composite preparation

PDMS prepolymer and curing agent (Sylgard 184, Dow Corning) were manually mixed (mixing ratio 10:1 by weight) and degassed for 1 h. Polyimide powder (P84, Evonik) was added to the PDMS mixture in different concentration, namely 10, 25, 50 and 100% into the

PDMS (i.e. from 0,1:1 to 1:1 of PI/PDMS ratio), then manually mixed for 10 minutes and degassed for 1 h. The mixture was poured into a dedicated PMMA mold and then cross-linked at 60 °C for 1 h. Membranes with thickness of 1 mm were removed from the mold and manually cut in 2 × 1 cm^2 pieces.

Morphological/Structural Characterization

Electron microscopy analysis was performed with a Field-emission scanning electron microscope (FESEM Supra 40, Zeiss) equipped with a Si(Li) detector for Energy-dispersive X-ray spectroscopy.

The structure of the LIG was investigated by Transmission Electron Microscopy with a FEI Tecnai G2 F20 Super-Twin operated at 200 kV acceleration voltage. Concerning sample preparation, the LIG structure was detached by the substrate through sonication and subsequently drop-casted on a lacey carbon on copper TEM grid.

Raman measurements

Raman spectroscopy was performed by means of a Renishaw InVia Reflex micro-Raman spectrometer, equipped with a cooled CCD camera. A 514 nm laser source was used, focused through a 50X microscope objective, with backscattering light collection.

Electrical characterization

Electrical characterizations have been performed with a Keysight B2912A Source/Measure unit in an ISO 6 cleanroom under controlled humidity and temperature conditions. Laser written samples were mounted on a probes station and current-voltage (I-V) characteristics have been measured in two terminal configuration with a scan rate of 300 mV/s in the range -5 V; +5 V. Sample resistances R have been extracted from the I-V curves and sheet resistances have been calculated as $R_s = R \cdot \frac{W}{L}$ being W and L respectively the widths and lengths of laser written samples.

Mechanical properties (deformation) and strain gauges

Mechanical properties of the samples were tested with a Universal Testing System (Instron 3365). The bare PDMS and the PDMS-Pi samples were prepared by casting slice of 40 mm length, 5 mm width and 1 mm thickness. The piezoresistive measurements were conducted on LIG samples written on 50% PDMS-PI composite. The two extremities of LIG lines were glue to copper wires using silver paste. The electrical measurements were done with a Keithley 2635A sourcemeter. For the tensile strain was used the previous described Universal Testing System, while for the bending deformation, the samples were bended over cylinders with different radii. The temperature measurements were conducted in a electrical hoven (Memmert 30-1060) with opening for the electrical cables.

Supercapacitors characterization

The SC was probed through metallic wires bonded on the electrodes thanks to silver conducting paste purchased by RS components. The wires were placed on the contact pads and covered with the silver paste, cured at 60°C for 1h. The electrolyte, Na_2SO_4 1M, was placed over the interdigitated terminals in soaked filter paper in order to avoid any contact with the silver bonds. Two electrodes measurements were performed with Metrohm Autolab Potentiostat/Galvanostat equipped with impedance module FRA32M at room temperature. Three main techniques were run to characterize the device performance: Cyclic Voltammetry (CV), Galvanostatic Charge and Discharge (CDG) and Electrochemical Impedance Spectroscopy (EIS). The active area considered for the specific capacitance of the cell was the one underneath the separator, carefully designed according to the interdigitated portion of the electrodes. The device was tested in bending condition by means of only CV.

For the CVs the potential was let sweep in a 0.8V potential window at five different scan rate: 20, 50, 100, 200 and 500 mV s^{-1}. During bending tests, we scanned at 100 mV s^{-1}. For CDGs we imposed four current densities: 1, 2, 5 and 10 µA cm^{-2}. Finally, for the EIS we set up a scan from 1MHz down to 10mHz with a probe signal of 5mV peak.

Apart from bending and strain tests, device specific capacitance was computed according to

$C_S = I\,\Delta t_d / (\Delta V\,S)$ [F cm^{-2}] (1)

in which I is the constant current, Δt_d the discharge time, ΔV the respective voltage variation and S the active area covered by the electrolyte. Concerning calculations from CV measurements for bending tests, we used the relation

$C_S = int[i_d(t)]dt / (\Delta V\,S)$ [F cm^{-2}] (2)

where $i_d(t)$ is the discharge current profile, ΔV the voltage window and S the active area. Energy and power were computed applying

$E_S = ½\ (1/3600)\ C_S\,\Delta V^2$ [Wh cm^{-2}] (3)

$P_S = E_S / (\Delta t_d/3600)$ [Wh cm^{-2}] (4)

in which C_S is the one computed from CCCD tests and the other quantities are related to them.

3. Results and discussion

3.1 Physico-chemical characterization of LIG/PI composite

The effect of PI powder addition into the PDMS matrix was investigated by field-emission scanning electron microscopy. **Figure S1** in the supporting information shows the cross-sections of the composites obtained varying the PI powder concentration: 10, 25, 50 and 100% into the PDMS (i.e. from 0,1:1 to 1:1 of PI/PDMS ratio). Micrometric agglomerates of PI powder are clearly observable in cross-section images: they appear as complex features against the low-contrast background related to the PDMS matrix. High-resolution images (see Supporting Information) confirm that the agglomerates are constituted by PI powder, since they exhibit the same morphology as the pristine powder. It is interesting to notice that with 100% loading the PDMS matrix is almost completely filled with PI powder, thereby dramatically affecting the mechanical properties of the composite in favor of a maximization of graphitizable material.

Before the investigation of the laser-writing process on the PDMS-PI composites, a preliminary study of the effects of such process on PDMS and PI separately was conducted.

It is noteworthy to underline that this represents the first attempt, to the best of our knowledge, to laser-write an elastomeric substrate in order to obtain a conductive graphene-based path. Moreover, also PI powders were never converted in LIG nor alone or in a composite matrix. The writing parameters were set up based on the previous experience on PI substrates.[18]

The FESEM analysis allows to verify the morphological evolution of the PI powder (**Figure 1**). Due to the obvious 3D profile of the non-standard substrate the laser-spot cannot be perfectly focused during the whole writing process but it is possible to recognize the typical LIG arrangement among partially sintered PI particles. For what concerns the PDMS matrix, it is not possible to obtain LIG using the range of writing parameters investigated for PI. This can be explained considering the molecular structure of PDMS, with a siloxane chain and very low amount of carbon mainly in form of methyl groups. As shown in Figure 1, the written area on PDMS results into a porous network constituted of nanoparticles. This direct laser synthesis of highly porous nanostructured silica layer can be further investigated for possible application in microfluidic devices or drug delivery applications.[19-20]

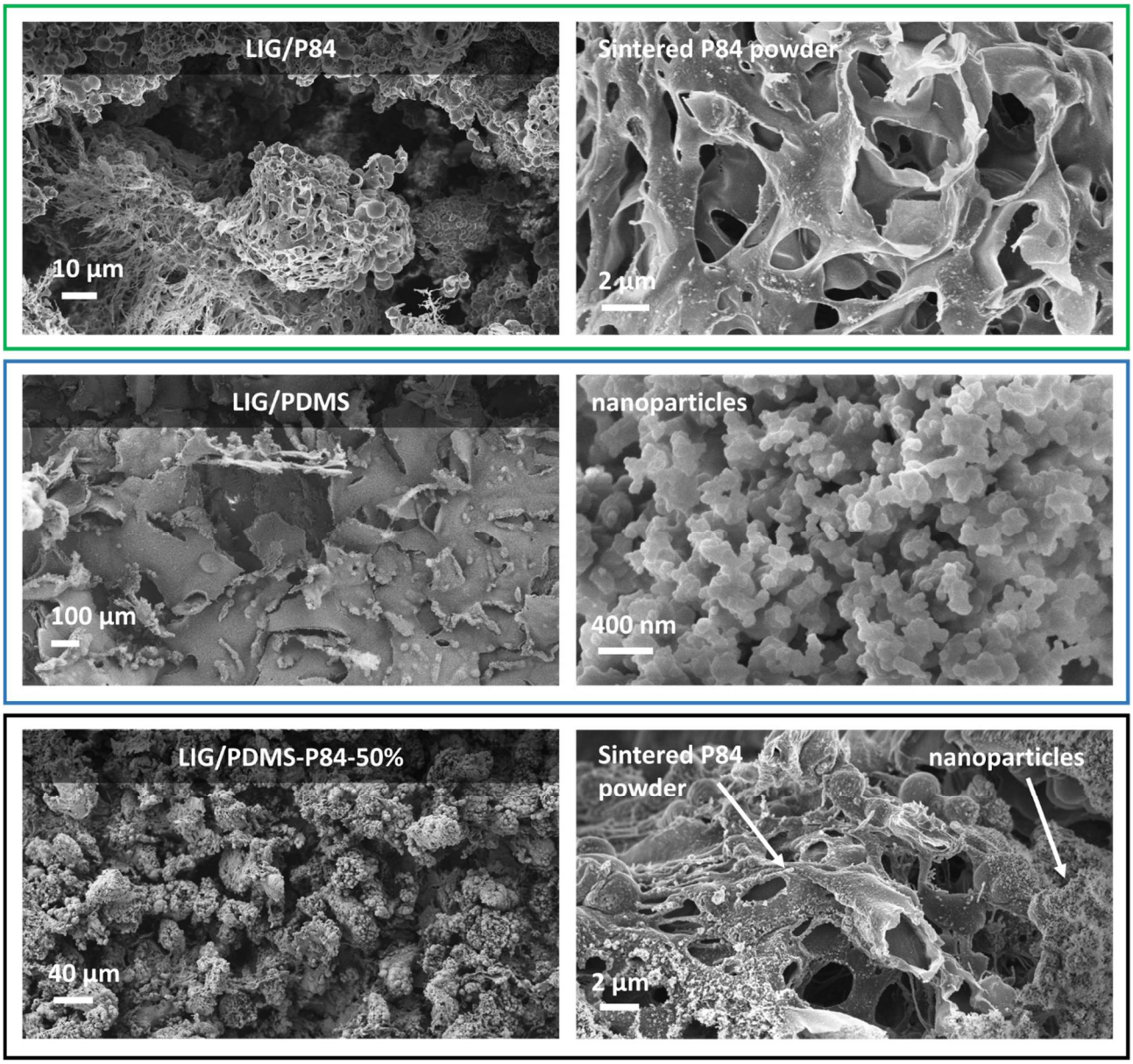

Figure 1. FESEM micrographs showing the top morphology of PI powder, PDMS and PDMS/PI composite after laser writing at different magnifications.

Figure 1 provides representative FESEM images of the obtained LIG after the laser-writing process, starting from PDMS loaded with 50% PI powder. Low-magnification images show that the typical 3D porous morphology of LIG is obtained. At the nanoscale, the sample exhibits a complex morphology based on two basic constituents: (i) walls with micrometric holes, resulting from the previously mentioned sintering of PI particles, (ii) nanoparticles resulting from the processing of PDMS.

This result is confirmed for all the different starting loadings (10%, 25%, 50%, 100%), as shown by FESEM analysis provided in the Supporting Information. The concentration of nanoparticles characteristic of laser-written PDMS is coherently higher for the samples with lower PI loading.

A first evidence of PI graphenization in the elastomeric matrix can be obtained through Raman spectroscopy. The Raman spectra for PDMS/PI composite (50% in weight of PI particles) written with different laser power are reported in **Figure 2**.

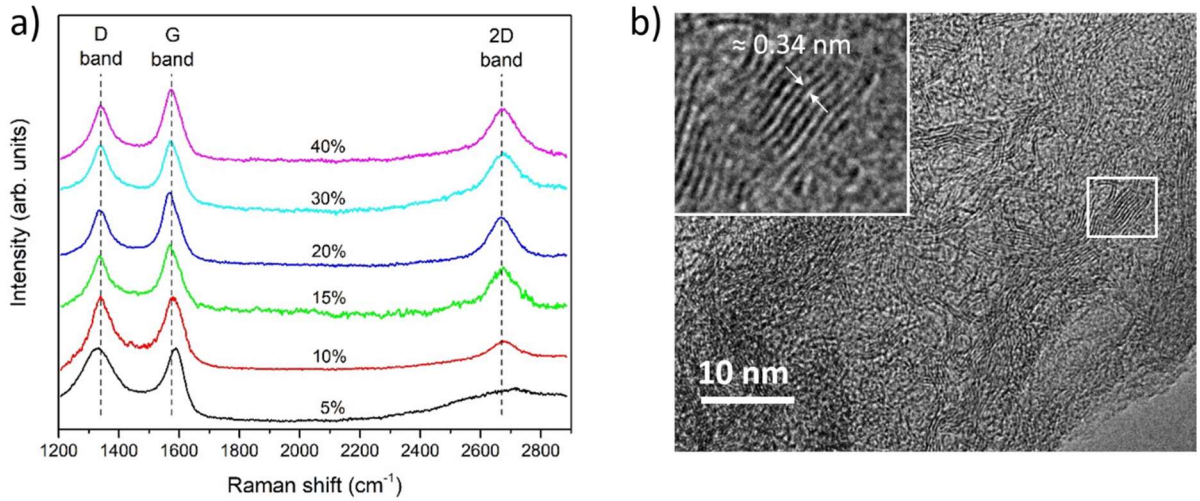

Figure 2. a) Raman spectra for LIG on PDMS/PI composite (50% in weight) ~~for~~ obtained with laser power between 5% and 40%. b) provides a high-magnification TEM image of the sample fabricated at 40% laser power. The inset provides a direct visualization of the layered structure.

The measured spectra show in all cases the typical features of few-layer graphene: the D band at ~1350 cm^{-1}, related with the formation of defects, vacancies and bent sp2 bonds, the G band at ~1580 cm^{-1}, originating from a first-order inelastic scattering process involving the degenerate iTO and iLO phonons at the G point (E2g mode) and finally the 2D peak at ~2700 cm^{-1}, the second harmonic of the D band. More in detail, Raman spectroscopy can provide some preliminary insights on the degree of graphenization of the structures during the laser writing process, as a function of the writing parameters. In fact, to study the degree of graphenization, the analysis of the intensity ratio between the D and the G peaks (I_D/I_G) can be performed. It is known from the Tuinstra–Koenig relationship that such ratio is inversely

proportional to the in-plane crystallite size, giving a preliminary view on the effectiveness of the laser treatment in the formation of the graphitic domains.[21] From the reported spectra, the optimal conditions were found for laser writing at 20% power, showing a minimum value of 0.72 ± 0.07 for I_D/I_G ratio. In these conditions, the 2D peak shows a well-defined, symmetric behavior, similar to the one obtained for ordered graphitic materials like turbostratic graphite. For lower laser power, the graphenization is probably incomplete, as also witnessed by a very weak 2D band and a I_D/I_G ratio of 1.0 ± 0.1 for 10% power. Instead, for higher power the defectiveness of the material increases again, and the I_D/I_G ratio reach a value of 0.79 ± 0.08 for 40% power.

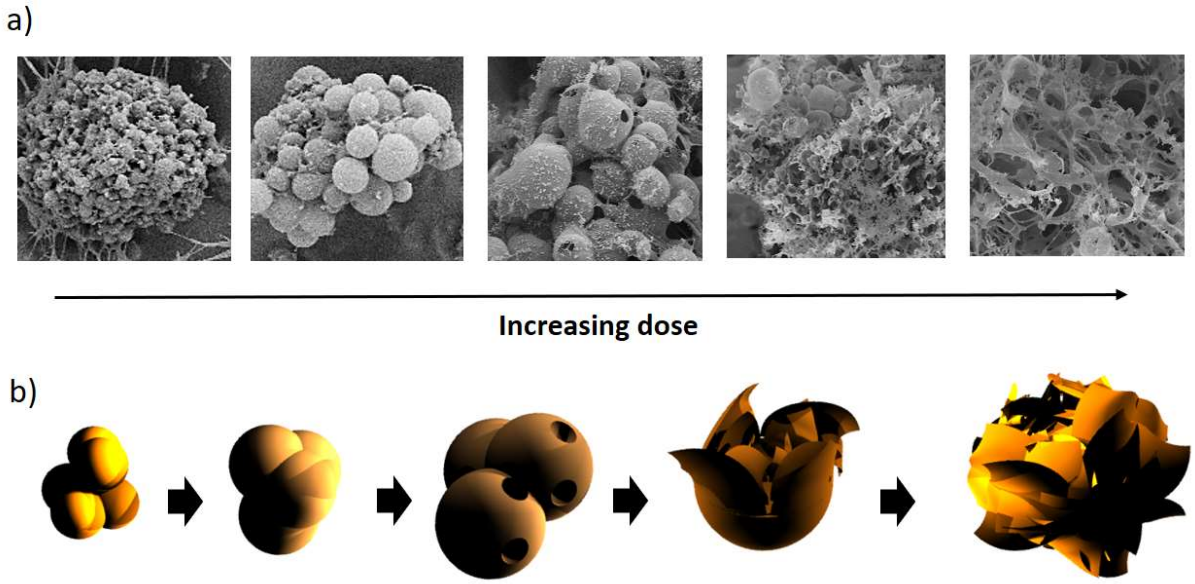

Figure 3. FESEM images (a) showing the evolution of the PI particles morphology at different conversion stages into LIG and respective 3D rendering (b).

Further structural information is acquired through TEM characterization: figure 2b provides results obtained on LIG fabricated on PDMS/PI composite (50%) with 40% lase power. TEM images provide a direct visualization of the structure of the LIG, which is constituted by a disordered arrangement of randomly oriented few-layer graphene features, with characteristic 0.34 nm interplanar spacing of the (002) family of planes. These findings are in accordance with LIG structures previously reported in the literature [https://doi.org/10.1002/adma.201803621, https://doi.org/10.1021/acs.accounts.8b00084].

Since the PI particle agglomerates have variable dimensions and are spatially distributed at different depths in the elastomeric matrix, at the end of the laser-writing process it is possible

to recognize on the surface of the PDMS/PI composite different degrees of conversion of PI powder into LIG. Indeed, based on their position in *z*, they are more or less out of focus with respect to the laser beam, a condition that corresponds to a different dose of energy (fluence) transferred to them (a critical fluence of ~5.5 J/cm^2 was required to obtain LIG on PI).[22] **Figure 3**a collects SEM images of PI particles initially identical to unwritten particles and increasingly converted to LIG. The mechanism proposed for this conversion is schematized in Figure 3b: laser irradiation locally raises the temperature of the particles, causing chemical bonds to break (graphenization step due to atoms rearrangement) and the sublimed atoms recombine into gaseous products bloating the PI particle. Then gases way out of the structure through the generation of holes finally resulting in a 3D foam-like graphene-based structure. Mechanical properties of the samples have been investigated trough tensile tests to evaluate the effect of the dispersion of the PI particles into the PDMS matrix. PDMS samples and its composites with dispersed 25, 50 and 100% in weight of PI particles were tested stretching up to the breakpoint (**Figure 4**a).

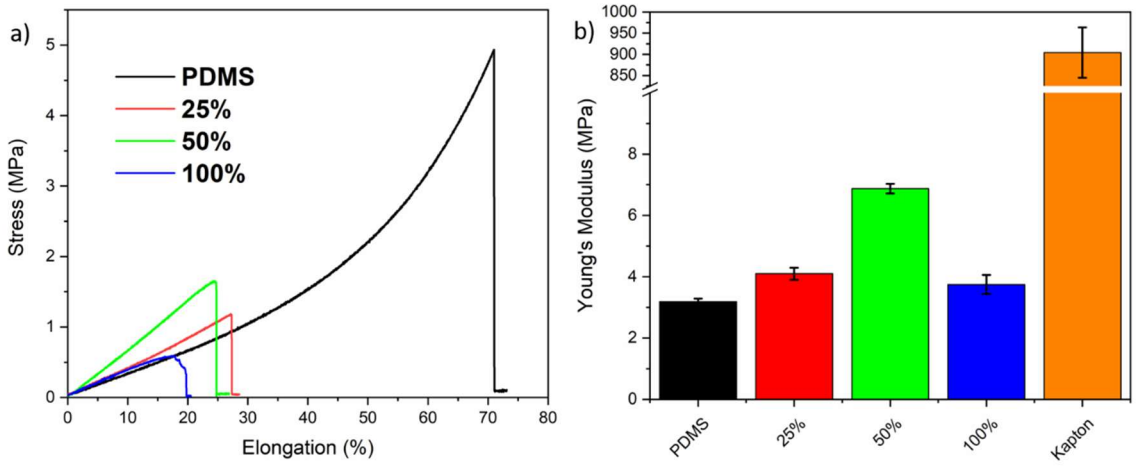

Figure 4. a) Stress-strain curves up to breakpoint for the bare PDMS and the PDMS-PI composite. b) Comparison of the Young's modulus of the bare PDMS, the PDMS-PI composite and the Kapton. The reported values were obtained by averaging five different measurements for each type of sample.

The Young's modulus of the samples was extracted from the slope of the first part of the stress-strain curves which shows a linear trend. The addition of the polyimide particles

reduces the breakpoint of the samples with respect to the bare PDMS. As expected, the more we increase the particles content, the more the breakpoint is reduced. Anyway, the elastic properties of the samples are still maintained as can be observed from the values of the Young's modulus. The addition of PI particles up to 50% increases the Young's modulus up to twice the PDMS one, since the polyimide particles acts as reinforcement, as shown in Figure 4b. Instead the Young's modulus is reduced in the samples with 100% content, because they presented a lot of voids inside the composite, since it was not possible in the curing step to remove all the air-bubble trapped during the preparation of the sample. For all the samples the Young's modulus remained around few MPa guarantee the flexibility and stretchability needed for both application as strain sensor and supercapacitors. Samples of PDMS-PI composite with LIG lines written on the surface were also tested and no variations of the mechanical properties was observed (see Supporting Informations). This behavior was expected since the thickness of the part of composite modified by the LIG process (few tens of μm) is negligible with respect of the whole composite thickness (around 1 mm). As a comparison we also reported the mechanical properties of the Kapton foil, which is the standard substrate for LIG; thin foil of Kapton can be easily bend, but with respect to the PDMS-PI composites they are not stretchable.

Electrical measurements were performed revealing the electrically conductive characteristic of the laser-written composite. The laser parameters and the PI powder concentration were tuned in order to reduces as much as possible the resistive contribution of the LIG electrodes. **Figure 5**a collects the results of the electrical characterization in terms of sheet resistance (an image of the test pattern for electrical characterization is reported in the inset) which is the standard figure of merit analyzed in LIG devices.

From the isosurface plot it is possible to see how, at a fixed laser power, by increasing the pulse frequency of the laser the sheet resistance decreases of two order of magnitude.

Similarly, the increase of laser power at a fixed pulse frequency, positively influence the conductivity reducing again the sheet resistance.

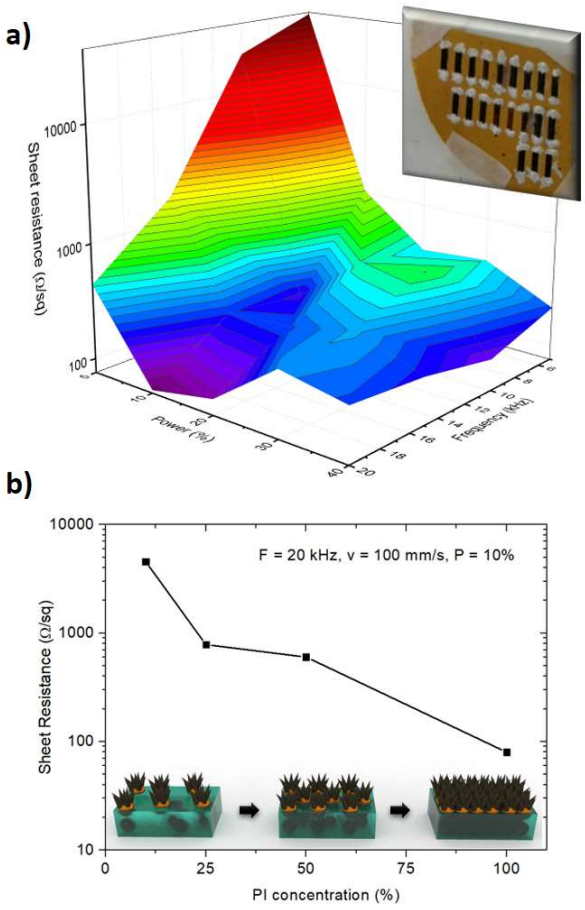

Figure 5. Sheet resistance of the laser-written PDMS/PI varying laser parameters (a) and PI concentration (b).

All these results, even if not obvious, follow trends similar to previous reports on LIG on PI foil.[15, 18] The novel finding, intrinsically due to the composite nature of the substrate under investigation, concerns the effect of the amount of PI powder into the PDMS matrix. Increasing particle concentration, the resulting LIG become more and more conductive due to the higher interconnection among the flakes of the converted particles, as schematically represented in Figure 5b.

3.2 Multifunctional electrodes for flexible device

The present findings reveal that laser written PDMS/PI substrates are sufficiently electrically conductive and mechanically stable to be used as multifunctional electrodes for flexible electronics. For this reason, two kind of prototypes have been designed, fabricated, and characterized to illustrate the possible applications in this research field.

2.2.1 LIG on PDMS/PI for strain gauge

Firstly, we investigated the piezoresistive properties of the LIG on PDMS-PI composite for its application as strain gauge. For this purpose, we prepared two different devices made with LIG on PDMS-PI composite, one with a single line pattern and one with a serpentine pattern to reproduce the standard design of commercial strain gauges. Indeed, the serpentine pattern maximize the electrical resistance variation, because of the elevated line length contained in a small area. The two devices were written on the 50% PDMS-PI composite.

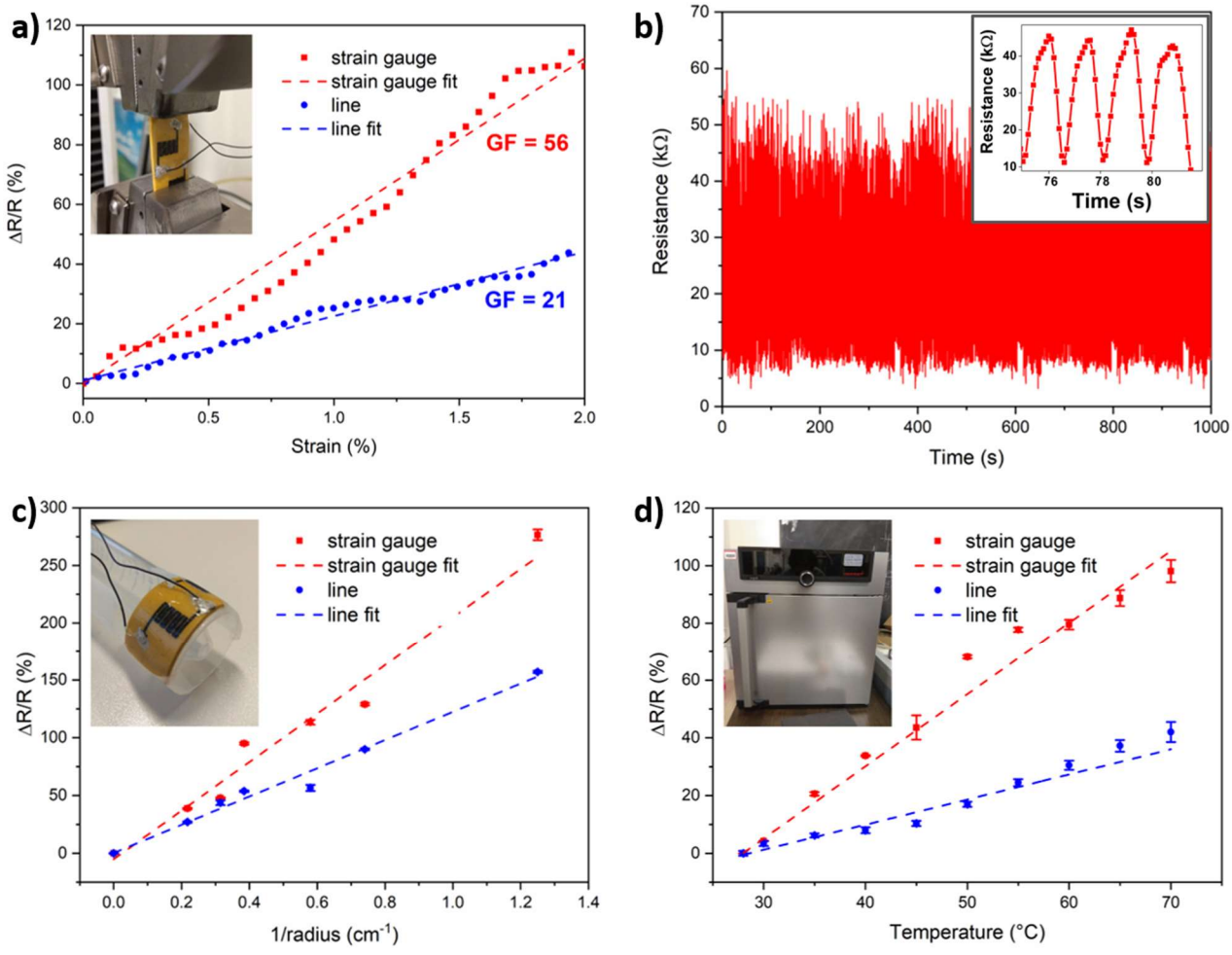

Figure 6. a) Piezoresistive response under linear strain of LIG devices with strain gauge and line pattern. b) Stability of the electrical resistance response of the strain gauge device under cyclic linear deformations. A zoom of the cycles is reported in the inset. c) Piezoresistive response of LIG devices as a function of the bending radius. d) Electrical resistance variation of the LIG devices for different working temperature.

This composition represents a compromise between a low sheet resistance, even if higher than the 100% PDMS-PI composite one, and a higher stretchability and flexibility, which is worse in the 100% PDMS-PI because of the trapped air bubbles. The devices were tested by elongating them with a universal testing machine as shown in **Figure 6**a. As expected they showed a positive pressure coefficient of resistance (PPCR) effect with an increase of the electrical resistance when subject to deformation, which is typical of system with 1D or 2D filler such as carbon nanotube or graphene.[23-24] In our devices, with the application of the tensile strain, the flakes composing the LIG structures are distanced reducing the contact points between them and thus damaging the conductive network. The electrical resistance variation showed a linear trend and is much higher in the strain gauge configuration with respect to the line one. The gauge factor defined as the ratio between the resistance variation and the strain ε ($GF=(\Delta R/R)/\varepsilon$)[25-26] is 56 for the strain gauge configuration and 21 for the line one. These values are in line with the piezoresistive composite sensors based on graphene sheets, which presents GF between 20 and 200,[27-28] and is comparable to the few other works on LIG strain sensor with GF around 50.[11] The main advantage of our device is the direct write with the laser on a flexible substrate, while the other works in literature are based on LIG devices written on Kapton substrate and then eventually transferred in PDMS matrix. When the application needs very small deformation (few micrometer) like acoustic transducers, the device was directly used on Kapton substrate.[29] Otherwise the LIG pattern was transferred from Kapton to PDMS substrate with the risk of damaging the conductive network.[11, 30] Similarly to other graphene based sensors, our device works very well for small strain up to 2%.[31-32] Above this limit the conductive network between the flakes of LIG get strongly damaged with a fast decreasing of contact points among the flakes and the sensor response is not anymore linear. Also in this strain range, the device presents a very good

response stability as evidenced by the fast-cyclic deformation (1 cycle every 2 s) presented in Figure 6b for the strain gauge configuration, obtained for deformation around 5%.

The strain devices were also tested in bending configuration reporting a noteworthy response. Both the strain gauge and the line configuration showed a linear increasing of resistance when bend over cylinder of smaller radii. As expected the strain gauge configuration reported a higher response with respect to the line one. During the bending, the top part of the LIG pattern is subjected to a tensile stress and thus the flakes are distanced reducing the conductive network of the sensor. The bottom part of the LIG in contact with the PDMS is subjected to a compressive stress and then the flakes are moved close to each other increasing the local conductive network. Since the sensors experienced an increase of electrical resistance, the global effect is dominating by the top part. The presence of the compressive stress in the bottom part guarantees the maintaining of a conductive network also for large deformation (i.e. small bending radii) and thus enlarges the operative range of the sensors with respect of the previous experiment of linear strain (Figure 6a). Another fundamental parameter for the strain sensor is the temperature dependence. All the resistive strain sensors presented a variation of their response with the temperature related to the expansion coefficient of the constituent materials. Piezoresistive sensors fabricated with PDMS based composite show a remarkable temperature dependence since the elevate thermal expansion coefficient of the polymer ($\delta L = 3.2*10^{-4}\ °C^{-1}$).[33-34] We tested both our devices in a temperature range between room temperature and 70°C and it was observed an increasing of the electrical resistance (Figure 6d). This variation is comparable to the linear deformation of around 2% presented in Figure 6a and is compatible with the thermal expansion of the polymer in the applied temperature range. Slight variation can be accounted to the neglected thermal expansion of the powder which has a small impact on the whole sample since it does not constitute a continuous network. However, the presence of an elevate resistance variation with the temperature does not represent a limitation for the application of our LIG devices on

PDMS-PI composite since this dependence can be easily compensated with the electronics or using dummy sensors.

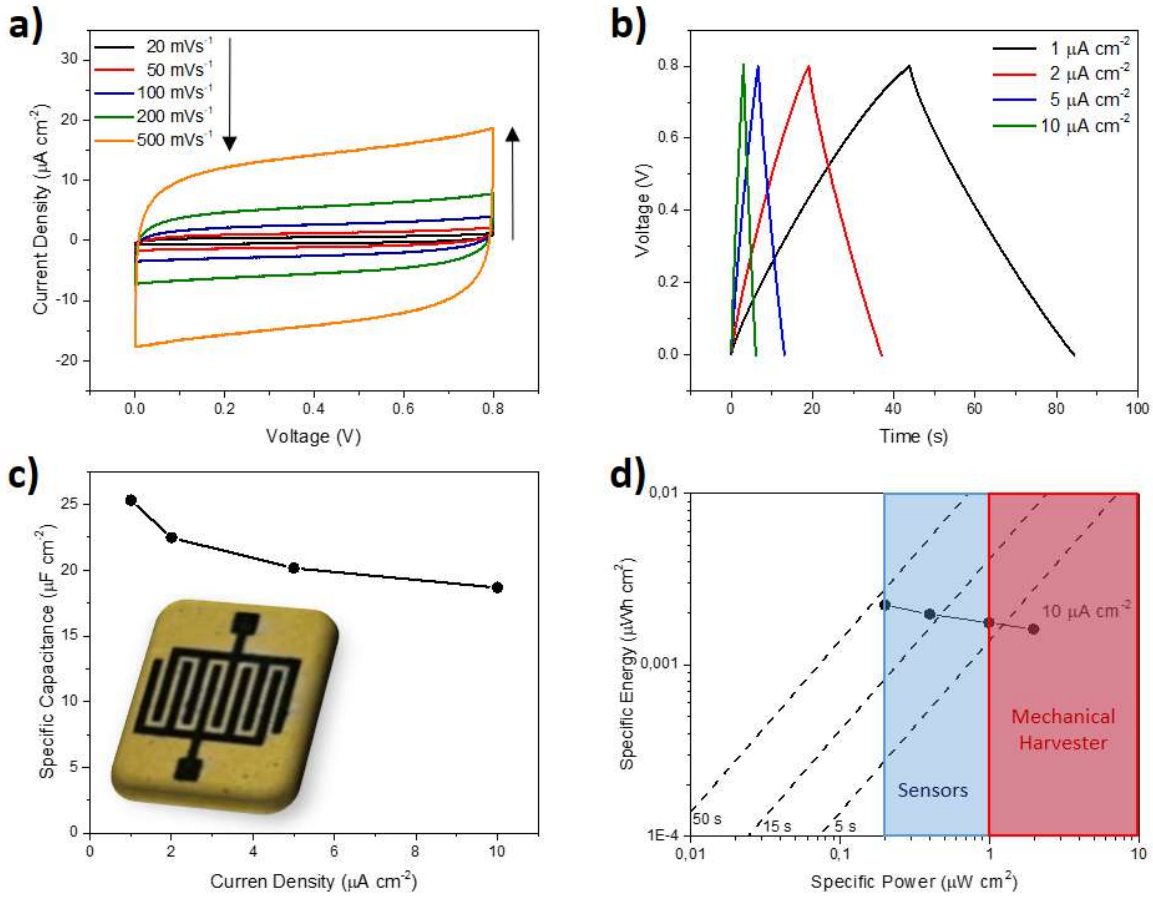

Figure 7. Two electrodes electrochemical characterization of the SC in 1M Na_2SO_4: a) CV performed at several scan rates. b) CDG performed at several current densities. c) Cell capacitance and d) Ragone plot derived from CDG tests.

2.2.2 LIG on PDMS/PI for supercapacitor

The second prototype fabricated to demonstrate the multifunctional nature of the proposed material is a supercapacitor. As stated in the introduction, LIG has been largely investigated as flexible electrode for supercapacitor fabrication. Several materials have been converted into LIG ranging from the more traditional aromatic polymers to more uncommon ones such as wood or edible substrates.[16, 35] To the best of our knowledge, this is the first study of an electrochemical energy storage device obtained through laser writing directly on elastomeric substrate.

We chose the optimal writing parameters coming from previous analysis (see Figure 5) in order to achieve the best electrode conductivity. We patterned the device according to an interdigitated architecture of five pins per electrode as depicted in the inset of **Figure 7**a. Devices were characterized in 1M Na_2SO_4 electrolyte solution by means of common electrochemical techniques such as Cyclic Voltammetry (CV), Galvanostatic Charge and Discharge (CDG) and Electrochemical Impedance Spectroscopy (EIS). We performed then bending tests under CV analysis.

We performed CV tests by sweeping the scan rate at the values 20, 50, 100, 200 and 500 mV s^{-1} and limited the potential window to 0.8V to avoid the onset of water-splitting redox current, as shown in Figure 7a. All the CVs recorded show an ideal rectangular shape, mirror-symmetric with respect to the horizontal axis and remain close to ideal and mirror-symmetric even at higher scan rates. The rectangular shape of the CV profiles is proper of Electrical Double Layer Capacitors (EDLCs). Then we run galvanostatic test (Figure 7b) at different current densities (1, 2, 5 and 10 μA cm^{-2}) to access device specific capacitance and build the Ragone plot, reported in Figure 7c and Figure 7d respectively. The device showed a small IR-Drop over the whole range of current values and very good rate capability with 20% retention, as shown in Figure 7c. Furthermore, the triangular CDG profiles with linear charge and discharge characteristics is a further confirmation of the EDL charge storage mechanism of the fabricated supercapacitor.

The obtain energy storage performances are in line with other results reported in the literature about microsupercapacitors even if lower than LIG-based devices.[5, 36-38] This is mainly due to the lower conductivity and available surface area of the obtained electrodes since only a part of the written polymer incurs in graphenization with respect to fully dense aromatic substrate previously reported. However, it is worthy to underline that this approach allows for the fabrication of a binder-free and current collector-free material. Moreover, the performance can be easily overcome by post-processing of the written electrodes. Indeed, rarely LIG was

used alone as material for supercapacitor fabrication and several strategies have been proposed in the last years to improve its specific capacitance, energy and power density by decorating the carbon-based network with pseudocapacitive materials.[9]

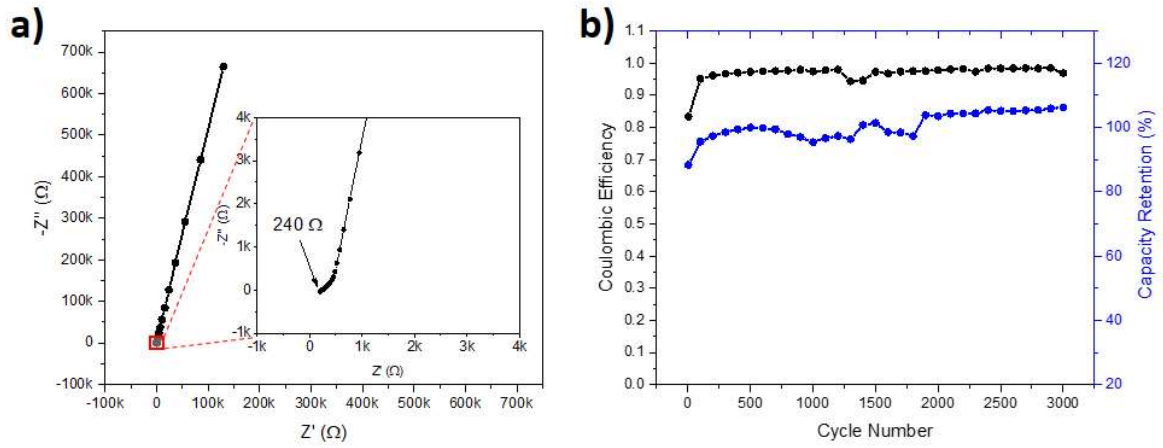

Figure 8. Two electrodes electrochemical characterization of the SC in 1M Na_2SO_4: a) EIS performed at V_p = 5mV from 1Mhz down to 10mHz b) Cyclic stability performed at 100 mV s^{-1} and derived capacity retention.

Another important consideration relies on the final application of the microsupercapacitors. Among the sea of opportunities of these energy storage devices, one foreseen potential application is related to their integration with energy harvesters and microelectronics to realize self-powered and maintenance-free sensing systems able to answer to the requirement of the Internet of Things (IoT). The most common energy harvesting technologies can convert energy into electricity exploiting different mechanisms such as photovoltaic, piezo and triboelectric, thermoelectric and many others.[39] However, most of the energy sources can provide only intermittent generation and so the energy storage become essential.[40-41] Shen et al. in a recent review deeply analyze the problem providing an overview of the performance requirements of such applications in order to evaluate practical microsupercapacitors integration.[42] Comparing their analysis with the here reported results, we found out that our device can be a good candidate in this field matching in particular the energy harvested by mechanical generators to power several portable sensors, as underlined by the red and blue area in the Ragone plot (see Figure 7d).

EIS was also performed in order to characterize interfacial and transport properties, the Nyquist plot is reported in **Figure 8**a. The high ESR = 240 Ω (Z' @ Z"=0) can be attributed completely to the high resistivity LIG electrode. Nonetheless, this value confirms the small sensitivity to current density variations in CDG tests thus the good rate capability. The absence of semicircle confirms the EDLC interface. Moreover, the device showed constant phase shift typical of a capacitive element with constant phase shift of 80° up to 10 Hz. Cyclic stability was performed with CV tests at 100 mV s^{-1}. The results are shown in Figure 8b in which it can be appreciated a constant, high, Coulombic Efficiency for 3000 cycles. The increasing trend in the capacity retention can be ascribed to electrodes wettability slowdown by the combination of two effects: hydrophobicity of both PDMS and LIG. During cycling the wettability slowly increase inducing a monotone rising trend.

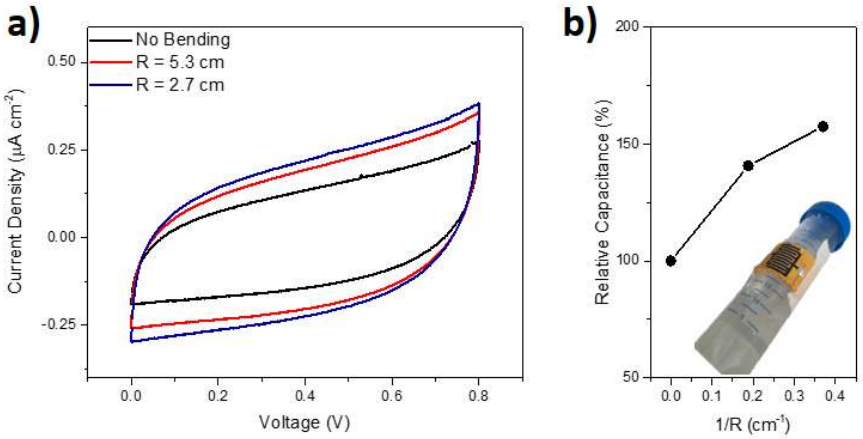

Figure 9. a) CVs and b) calculated relative capacitance at different curvature radii (flexible supercapacitor is shown in the inset).

Finally, we performed bending tests to study the capacitance stability of the device under bending conditions. The CVs at 100 mV s^{-1} at two different bending radii (5.3 cm and 2.7 cm) are shown in **Figure 9** and compared with the flat condition. We observed a rise of about 60% in device capacitance with stable rectangular shape versus the inverse of the bending radius. In our opinion, this might be due to an improved electrodes-electrolyte interface induced by the bending. However, the slope of the CV slightly increases at higher bending angles. As

well known in the literature,[43] this trend can be explained by an increase in the device series resistance. Moreover, it is worthy to observe that the device was able to retain coulombic efficiency higher than 90% even at the harsher bent condition.

4. Conclusion

A novel elastomeric composite based on PDMS network and Polyimide powder has been proposed as substrate for multifunctional electrodes obtained by laser writing induced graphitization. The obtained composite has been characterized revealing tunable mechanical properties and strong dependence of the PI powder content on the graphitization process. The pulsed laser beam was found to induce an expansion of the PI particle during photo-thermal conversion into LIG finally resulting in a sponge-like morphology. Additionally, various laser writing parameters have been investigated in order to maximize the conductivity of the graphene-based material. The LIG obtained on PDMS/PI composite has been used ad electrodes for flexible electronic application focusing the attention on two class of devices: namely strain gauges and supercapacitors. Both the devices show performances comparable to similar state-of-the-art devices with an obvious advantage introduced by the easy processability of the proposed composite. This paves the way to simple fabrication of LIG-based complex geometries overcoming the actual limitation of introducing conductive paths onto three dimensional objects.

Supporting Information

Supporting Information is available online or from the author.
Additional FESEM characterizations.

Acknowledgements

M. Parmeggiani and P. Zaccagnini equally contributed to this work.

References

(1) Kim, S. J.; Choi, K.; Lee, B.; Kim, Y.; Hong, B. H., Materials for Flexible, Stretchable Electronics: Graphene and 2D Materials. In *Annual Review of Materials Research*, 2015; Vol. 45, pp 63-84.
(2) Harris, K. D.; Elias, A. L.; Chung, H. J. Flexible electronics under strain: a review of mechanical characterization and durability enhancement strategies. *Journal of Materials Science* **2016,** *51* (6), 2771-2805, DOI: 10.1007/s10853-015-9643-3.
(3) Kim, D.; Yun, J.; Lee, G.; Ha, J. S. Fabrication of high performance flexible micro-supercapacitor arrays with hybrid electrodes of MWNT/V<inf>2</inf>O<inf>5</inf>nanowires integrated with a SnO<inf>2</inf>nanowire UV sensor. *Nanoscale* **2014,** *6* (20), 12034-12041, DOI: 10.1039/c4nr04138k.
(4) Peng, L.; Peng, X.; Liu, B.; Wu, C.; Xie, Y.; Yu, G. Ultrathin two-dimensional MnO<inf>2</inf>/graphene hybrid nanostructures for high-performance, flexible planar supercapacitors. *Nano Letters* **2013,** *13* (5), 2151-2157, DOI: 10.1021/nl400600x.
(5) Ye, R.; James, D. K.; Tour, J. M. Laser-Induced Graphene. *Accounts of Chemical Research* **2018,** *51* (7), 1609-1620, DOI: 10.1021/acs.accounts.8b00084.
(6) Lamberti, A.; Serrapede, M.; Ferraro, G.; Fontana, M.; Perrucci, F.; Bianco, S.; Chiolerio, A.; Bocchini, S. All-SPEEK flexible supercapacitor exploiting Laser-induced graphenization. *2D Materials* **2017,** *4* (3), DOI: 10.1088/2053-1583/aa790e.
(7) Clerici, F.; Fontana, M.; Bianco, S.; Serrapede, M.; Perrucci, F.; Ferrero, S.; Tresso, E.; Lamberti, A. In situ MoS<inf>2</inf>Decoration of Laser-Induced Graphene as Flexible Supercapacitor Electrodes. *ACS Applied Materials and Interfaces* **2016,** *8* (16), 10459-10465, DOI: 10.1021/acsami.6b00808.
(8) Song, W.; Zhu, J.; Gan, B.; Zhao, S.; Wang, H.; Li, C.; Wang, J. Flexible, Stretchable, and Transparent Planar Microsupercapacitors Based on 3D Porous Laser-Induced Graphene. *Small* **2018,** *14* (1), DOI: 10.1002/smll.201702249.
(9) Li, L.; Zhang, J.; Peng, Z.; Li, Y.; Gao, C.; Ji, Y.; Ye, R.; Kim, N. D.; Zhong, Q.; Yang, Y.; Fei, H.; Ruan, G.; Tour, J. M. High-Performance Pseudocapacitive Microsupercapacitors from Laser-Induced Graphene. *Advanced Materials* **2016,** *28* (5), 838-845, DOI: 10.1002/adma.201503333.
(10) Nag, A.; Mukhopadhyay, S. C.; Kosel, J. Sensing system for salinity testing using laser-induced graphene sensors. *Sensors and Actuators, A: Physical* **2017,** *264*, 107-116, DOI: 10.1016/j.sna.2017.08.008.
(11) Rahimi, R.; Ochoa, M.; Yu, W.; Ziaie, B. Highly stretchable and sensitive unidirectional strain sensor via laser carbonization. *ACS Applied Materials and Interfaces* **2015,** *7* (8), 4463-4470, DOI: 10.1021/am509087u.
(12) Tittle, C. M.; Yilman, D.; Pope, M. A.; Backhouse, C. J. Robust Superhydrophobic Laser-Induced Graphene for Desalination Applications. *Advanced Materials Technologies* **2018,** *3* (2), DOI: 10.1002/admt.201700207.
(13) Zhang, J.; Ren, M.; Li, Y.; Tour, J. M. In Situ Synthesis of Efficient Water Oxidation Catalysts in Laser-Induced Graphene. *ACS Energy Letters* **2018,** *3* (3), 677-683, DOI: 10.1021/acsenergylett.8b00042.
(14) Zhang, J.; Ren, M.; Wang, L.; Li, Y.; Yakobson, B. I.; Tour, J. M. Oxidized Laser-Induced Graphene for Efficient Oxygen Electrocatalysis. *Advanced Materials* **2018,** *30* (21), DOI: 10.1002/adma.201707319.
(15) Lin, J.; Peng, Z.; Liu, Y.; Ruiz-Zepeda, F.; Ye, R.; Samuel, E. L. G.; Yacaman, M. J.; Yakobson, B. I.; Tour, J. M. Laser-induced porous graphene films from commercial polymers. *Nature Communications* **2015,** *5*, DOI: 10.1038/ncomms6714.
(16) Chyan, Y.; Ye, R.; Li, Y.; Singh, S. P.; Arnusch, C. J.; Tour, J. M. Laser-Induced Graphene by Multiple Lasing: Toward Electronics on Cloth, Paper, and Food. *ACS Nano* **2018,** *12* (3), 2176-2183, DOI: 10.1021/acsnano.7b08539.

(17) Lamberti, A.; Clerici, F.; Fontana, M.; Scaltrito, L. A highly stretchable supercapacitor using laser-induced graphene electrodes onto elastomeric substrate. *Advanced Energy Materials* **2016,** *6* (10), DOI: 10.1002/aenm.201600050.
(18) Lamberti, A.; Perrucci, F.; Caprioli, M.; Serrapede, M.; Fontana, M.; Bianco, S.; Ferrero, S.; Tresso, E. New insights on laser-induced graphene electrodes for flexible supercapacitors: Tunable morphology and physical properties. *Nanotechnology* **2017,** *28* (17), DOI: 10.1088/1361-6528/aa6615.
(19) Slowing, I. I.; Trewyn, B. G.; Giri, S.; Lin, V. S. Y. Mesoporous silica nanoparticles for drug delivery and biosensing applications. *Advanced Functional Materials* **2007,** *17* (8), 1225-1236, DOI: 10.1002/adfm.200601191.
(20) Chen, Q.; MacCioni, G.; Sacco, A.; Ferrero, S.; Scaltrito, L. Fabrication of microstructures on glass by imprinting in conventional furnace for lab-on-chip application. *Microelectronic Engineering* **2012,** *95*, 90-101, DOI: 10.1016/j.mee.2012.01.007.
(21) Tuinstra, F.; Koenig, J. L. Roman spectrum of graphite. *The Journal of Chemical Physics* **1970,** *53* (3), 1280-1281.
(22) Duy, L. X.; Peng, Z.; Li, Y.; Zhang, J.; Ji, Y.; Tour, J. M. Laser-induced graphene fibers. *Carbon* **2018,** *126*, 472-479, DOI: 10.1016/j.carbon.2017.10.036.
(23) Lu, N.; Lu, C.; Yang, S.; Rogers, J. Highly sensitive skin-mountable strain gauges based entirely on elastomers. *Advanced Functional Materials* **2012,** *22* (19), 4044-4050, DOI: 10.1002/adfm.201200498.
(24) Stassi, S.; Cauda, V.; Canavese, G.; Pirri, C. F. Flexible tactile sensing based on piezoresistive composites: A review. *Sensors (Switzerland)* **2014,** *14* (3), 5296-5332, DOI: 10.3390/s140305296.
(25) Stassi, S.; Canavese, G.; Cosiansi, F.; Gazia, R.; Fallauto, C.; Corbellini, S.; Pirola, M.; Cocuzza, M. Smart piezoresistive tunnelling composite for flexible robotic sensing skin. *Smart Materials and Structures* **2013,** *22* (12), DOI: 10.1088/0964-1726/22/12/125039.
(26) Stassi, S.; Canavese, G.; Cauda, V.; Marasso, S. L.; Pirri, C. F. Evaluation of different conductive nanostructured particles as filler in smart piezoresistive composites. *Nanoscale Research Letters* **2012,** *7*, DOI: 10.1186/1556-276x-7-327.
(27) Wang, B.; Lee, B. K.; Kwak, M. J.; Lee, D. W. Graphene/polydimethylsiloxane nanocomposite strain sensor. *Review of Scientific Instruments* **2013,** *84* (10), DOI: 10.1063/1.4826496.
(28) Chen, J.; Zheng, J.; Gao, Q.; Zhang, J.; Omisore, O. M.; Wang, L.; Li, H. Polydimethylsiloxane (PDMS)-based flexible resistive strain sensors for wearable applications. *Applied Sciences (Switzerland)* **2018,** *8* (3), DOI: 10.3390/app8030345.
(29) Tao, L. Q.; Tian, H.; Liu, Y.; Ju, Z. Y.; Pang, Y.; Chen, Y. Q.; Wang, D. Y.; Tian, X. G.; Yan, J. C.; Deng, N. Q.; Yang, Y.; Ren, T. L. An intelligent artificial throat with sound-sensing ability based on laser induced graphene. *Nature Communications* **2017,** *8*, DOI: 10.1038/ncomms14579.
(30) Wu, Y.; Beker, L.; Karakurt, I.; Cai, W.; Elwood, J.; Li, X.; Zhong, J.; Zhang, M.; Wang, X.; Lin, L. In *High resolution flexible strain sensors for biological signal measurements*, TRANSDUCERS 2017 - 19th International Conference on Solid-State Sensors, Actuators and Microsystems, 2017; pp 1144-1147.
(31) Li, X.; Zhang, R.; Yu, W.; Wang, K.; Wei, J.; Wu, D.; Cao, A.; Li, Z.; Cheng, Y.; Zheng, Q.; Ruoff, R. S.; Zhu, H. Stretchable and highly sensitive graphene-on-polymer strain sensors. *Scientific Reports* **2012,** *2*, DOI: 10.1038/srep00870.
(32) Kang, D.; Pikhitsa, P. V.; Choi, Y. W.; Lee, C.; Shin, S. S.; Piao, L.; Park, B.; Suh, K. Y.; Kim, T. I.; Choi, M. Ultrasensitive mechanical crack-based sensor inspired by the spider sensory system. *Nature* **2014,** *516* (7530), 222-226, DOI: 10.1038/nature14002.

(33) Li, Y. Challenges and Issues of Using Polymers as Structural Materials in MEMS: A Review. *Journal of Microelectromechanical Systems* **2018,** *27* (4), 581-598, DOI: 10.1109/jmems.2018.2837684.
(34) Stassi, S.; Canavese, G. Spiky nanostructured metal particles as filler of polymeric composites showing tunable electrical conductivity. *Journal of Polymer Science, Part B: Polymer Physics* **2012,** *50* (14), 984-992, DOI: 10.1002/polb.23091.
(35) Ye, R.; Chyan, Y.; Zhang, J.; Li, Y.; Han, X.; Kittrell, C.; Tour, J. M. Laser-Induced Graphene Formation on Wood. *Advanced Materials* **2017,** *29* (37), DOI: 10.1002/adma.201702211.
(36) Yoo, J. J.; Balakrishnan, K.; Huang, J.; Meunier, V.; Sumpter, B. G.; Srivastava, A.; Conway, M.; Mohana Reddy, A. L.; Yu, J.; Vajtai, R.; Ajayan, P. M. Ultrathin planar graphene supercapacitors. *Nano Letters* **2011,** *11* (4), 1423-1427, DOI: 10.1021/nl200225j.
(37) Liu, W. W.; Feng, Y. Q.; Yan, X. B.; Chen, J. T.; Xue, Q. J. Superior micro-supercapacitors based on graphene quantum dots. *Advanced Functional Materials* **2013,** *23* (33), 4111-4122, DOI: 10.1002/adfm.201203771.
(38) Beidaghi, M.; Gogotsi, Y. Capacitive energy storage in micro-scale devices: Recent advances in design and fabrication of micro-supercapacitors. *Energy and Environmental Science* **2014,** *7* (3), 867-884, DOI: 10.1039/c3ee43526a.
(39) Lee, J. H.; Kim, J.; Kim, T. Y.; Al Hossain, M. S.; Kim, S. W.; Kim, J. H. All-in-one energy harvesting and storage devices. *Journal of Materials Chemistry A* **2016,** *4* (21), 7983-7999, DOI: 10.1039/c6ta01229a.
(40) Scalia, A.; Bella, F.; Lamberti, A.; Gerbaldi, C.; Tresso, E. Innovative multipolymer electrolyte membrane designed by oxygen inhibited UV-crosslinking enables solid-state in plane integration of energy conversion and storage devices. *Energy* **2019,** *166*, 789-795, DOI: 10.1016/j.energy.2018.10.162.
(41) Cauda, V.; Stassi, S.; Lamberti, A.; Morello, M.; Fabrizio Pirri, C.; Canavese, G. Leveraging ZnO morphologies in piezoelectric composites for mechanical energy harvesting. *Nano Energy* **2015,** *18*, 212-221, DOI: 10.1016/j.nanoen.2015.10.021.
(42) Shen, C.; Xu, S.; Xie, Y.; Sanghadasa, M.; Wang, X.; Lin, L. A Review of On-Chip Micro Supercapacitors for Integrated Self-Powering Systems. *Journal of Microelectromechanical Systems* **2017,** *26* (5), 949-965, DOI: 10.1109/jmems.2017.2723018.
(43) Zaccagnini, P.; Serrapede, M.; Lamberti, A.; Bianco, S.; Rivolo, P.; Tresso, E.; Pirri, C. F.; Barbero, G.; Alexe-Ionescu, A. L. Modeling of electrochemical capacitors under dynamical cycling. *Electrochimica Acta* **2019,** *296*, 709-718, DOI: 10.1016/j.electacta.2018.11.053.